JCTC Journal of Chemical Theory and Computation

Article

Cite This: J. Chem. Theory Comput. 2019, 15, 4156−4169

pubs.acs.org/JCTC

Toward Automated Variational Computation of Rovibrational Resonances, Including a Case Study of the H_2 Dimer

Irén Simkó,[†] Tamás Szidarovszky,[†,‡] and Attila G. Császár*[,†,‡]

[†]Laboratory of Molecular Structure and Dynamics, Institute of Chemistry, ELTE Eötvös Loránd University, Pázmány Péter sétány 1/A, H-1117 Budapest, Hungary

[‡]MTA-ELTE Complex Chemical Systems Research Group, ELTE Eötvös Loránd University, Pázmány Péter sétány 1/A, H-1117 Budapest, Hungary

A general and semi-automatic technique, based on the complex absorbing potential (CAP) method, is developed for the variational computation and identification of rotational−vibrational resonance states. This technique is an extension of a method introduced by Tremblay and Carrington (*J. Chem. Phys.* **2005**, *122*, 244107), and it employs the damped eigenvectors of a CAP-modified Hamiltonian as a basis to describe resonance wave functions. The low-lying resonances of the weakly bound Ar·NO$^+$ complex are computed with the new and the traditional CAP techniques to test the new algorithm. As an additional, more challenging test case, the bound and resonance rovibrational states of the H_2 dimer, the latter with both negative and positive binding energies, are determined, corresponding to different rotational excitations of the H_2 monomers. Resonances above the first few dissociation channels of $(H_2)_2$ are computed with the new and the traditional CAP methods, revealing some new, assigned resonance quantum states not reported in the literature.

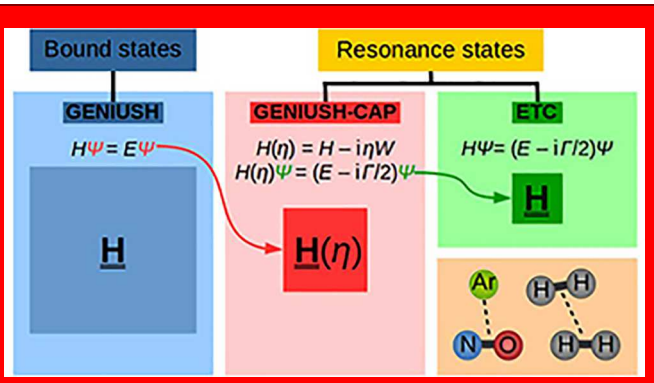

1. INTRODUCTION

Most molecular systems have a very large number of bound rovibrational states corresponding to their ground electronic state. In fact, even strongly bound triatomic systems, like isotopomers of the water molecule, with a first dissociation energy of about 40 000 cm^{-1},[1] possess rovibrational states on the order of a million.[2,3] In the era of the fourth age of quantum chemistry,[4] it has become possible to compute all these states[2,3] via solving the nuclear time-independent Schrödinger equation with the help of sophisticated variational and variational-like techniques.[4−6] These advanced bound-state computations do require a large amount of computer time but very little human intervention once the computations are set up properly.

It is also becoming more and more appreciated that all molecular systems exhibit a considerable number of rovibrational states with energies above the first dissociation limit, called resonance (often referred to as "quasibound") states. As an extreme case, for the Ar·NO$^+$ complex a large number of long-lived vibrational resonances have been found, even at 10 times the dissociation energy.[7] It is also known that resonance states of molecular complexes, like those of dimers, are often straightforward to measure due to their considerable lifetime. These findings are the consequences of the adiabatic separation of the dissociative motion from the rest of the nuclear motions (the separation is almost perfect for Ar·NO$^+$). In contrast to bound-state computations, determination of resonance states is not nearly as advanced. It is still necessary to improve these quantum-chemical methods, especially since most present-day techniques[8−11] require a considerable amount of human intervention to identify and characterize resonance states, and there are only a few past instances when resonances were computed via an automated technique.[12]

Resonance states of a system have higher energy than the corresponding dissociation limit (often the first one, but this may not always be the case, *vide infra*). However, since dissociation does not happen instantaneously, these states have well-defined, finite lifetimes, which can be very short but very long, as well, somewhat independently from the energy of the state. It is customary to describe resonance states by complex energies, $E^{res} = E - i\Gamma/2$ (in atomic units), where E is the state's energy (its position on the real axis), i is the imaginary unit, and Γ is the inverse lifetime of the state.

Unlike the wave functions of bound states, those of resonance states are not square integrable. Thus, the techniques employed for the variational solution of the time-independent nuclear Schrödinger equation, resulting in bound states,[4,6] cannot be utilized without modification for resonance states. There are at least four possible ways to compute rovibrational resonances: the stabilization method,[13] the complex coordinate scaling (CCS) method,[8,10] the complex absorbing potential (CAP) method,[9] and the use of scattering techniques.[14]

Received: March 30, 2019
Published: May 30, 2019

DOI: 10.1021/acs.jctc.9b00314
J. Chem. Theory Comput. 2019, 15, 4156−4169

In this Article, we consider possible improvements to the CAP methodology, moving toward the automatic determination and characterization of rovibrational resonances. The test system for the code development was chosen to be the $Ar{\cdot}NO^+$ complex, as the resonance energies of this weakly bound van der Waals (vdW) dimer have been studied with both variational and scattering techniques.[7] We then apply the new CAP-based technique to a more challenging test case, the computation of the special rovibrational energy-level structure of $(H_2)_2$.[15−20]

In the following section (section 2), we describe the general concepts of the method proposed for semi-automated rovibrational resonance computations. In the subsequent parts of the Article, we apply the technique developed to the $Ar{\cdot}NO^+$ and the $(H_2)_2$ complexes. The resonances of $Ar{\cdot}NO^+$ serve as a simple test of the method, while the more challenging case of the bound and resonance states of $(H_2)_2$ is investigated in more detail. After a general introduction to the two test systems in section 3, the details of the computations are described in section 4. The practical implementation of our semi-automated technique is presented in section 4.2.2. In section 5 we present the results for the two systems studied and discuss the performance of the new computational technique, mostly for $(H_2)_2$. Section 6 gives a summary of the most important findings of our study.

2. TOWARD AUTOMATED RESONANCE-STATE COMPUTATIONS

The CAP method[9] and one of its realizations, the GENIUSH-CAP code,[21] are suitable for the determination of rovibrational resonances of not only strongly bound molecules but also molecular complexes, such as $Ar{\cdot}NO^+$ and $(H_2)_2$. A major advantage of the CAP technique over the rival CCS technique is that CAP is general in the sense that it does not require the knowledge of the Hamiltonian in an analytic form and that it can be incorporated straightforwardly into discrete variable representation (DVR)[22,23] based numerical techniques as it changes only the potential-energy part of the Hamiltonian. Furthermore, the CAP approach has an advantage over the stabilization method, as well, as in the latter case one needs to perform a large number of variational bound-state computations, with different grid lengths along the dissociation coordinate, which can be expensive, while a CAP-based method may require only one costly bound-state computation and result in a much larger number of resonances.

Accordingly, the GENIUSH-CAP code[21] performs one expensive bound-state-type computation with the bound-state code GENIUSH[24,25] and the follow-up computation of the complex eigenvalue trajectories is inexpensive. Nevertheless, a huge drawback of the traditional CAP technique is that visual analysis must be used to identify cusps in the trajectories, corresponding to resonances. This involves a lot of human effort, and it also introduces some subjectivity when one decides whether a special curve feature is a cusp or not. Silva et al.[12] tested how to circumvent the visual analysis through an automatic analysis of the curvature of the CAP trajectories and the density of the points but in our own practice this method did not prove to be sufficiently robust.

In 2005, Tremblay and Carrington (TC)[26] suggested a method to simplify resonance-state computations based on a CAP. The basic idea of the TC method is as follows. In most CAP computations of rovibrational resonances the potential of the original Hamiltonian is modified in a way that basis functions suitable for bound-state computations can be employed, i.e., the outgoing part of the wave function is damped by the CAP. In the TC method one first determines the eigenvectors of a $\hat{H}(\eta_{\text{guide}})$ Hamiltonian,

$$\hat{H}(\eta_{\text{guide}}) = \hat{H} - i\eta_{\text{guide}}\hat{W} \tag{1}$$

and

$$\hat{H}(\eta_{\text{guide}})|\phi_k\rangle = E_k|\phi_k\rangle \tag{2}$$

where $\hat{W}$ is the CAP and η_{guide} is a suitable CAP strength parameter. Next one chooses a $\{|\phi_k\rangle\}$ basis by selecting a subset of these eigenvectors that resemble resonance-state wave functions (it is overly important to incorporate only those vectors into the basis which are small where the CAP function is large, and it is advantageous to divide the basis vectors into smaller groups based on the imaginary part of the complex energy). Finally, the E_i^{res} resonance energies are obtained as the eigenvalues of the original (unperturbed by the CAP) Hamiltonian matrix built in this basis, i.e.,

$$H_{kl} = \langle\phi_k^*|\hat{H}|\phi_l\rangle \tag{3}$$

$$\hat{H}\psi_i = E_i^{\text{res}}\psi_i \tag{4}$$

with the basis functions normalized such that $\langle\phi_k^*|\phi_l\rangle = \delta_{kl}$ (this comes from the properties of a projector introduced by TC). With the TC method one avoids the time-consuming search for cusps in the trajectories. Tremblay and Carrington tested the performance of the TC method on the $J = 0$ resonances of the HCO molecule (J is the total rotational quantum number).[26] They computed 90 resonance energies and widths in good agreement with results obtained via other techniques.

During the implementation of the TC method, we found the following issues with this procedure: (1) The choice of η_{guide} is not clear; fortunately, according to TC, the stability region is very broad. (2) It is unclear how one can find out which $|\phi_k\rangle$ vectors belong to resonances without inspecting an η trajectory, a step in the original CAP method we would like to avoid. (3) One of our test systems, the $(H_2)_2$ complex, has only a small number of resonances for a given dissociation channel; their number is not sufficient for forming a suitable basis.

As expected, the choice of the basis is key to the success of the TC method. To this end, we recapitulate some results of a paper by Riss and Meyer,[9] which describes the properties of eigenvalues and eigenvectors of the CAP-modified Hamiltonian in the case of a simple one-dimensional (1D) model. According to Riss and Meyer,[9] there are four types of complex eigenvalues, based on their position in the complex plane: (1) Some eigenvalues lie on the "45° axis", called the "rotated spectral string". Let us call these *string states*. One can show that string-state eigenvectors satisfy L^2 requirements, i.e., they are localized (see Appendix A of ref 9 for details). (2) There are eigenvalues below the "45° axis", these are called *diverging states*. They do not correspond to the poles of $(E - \hat{H})^{-1}$. (3) There are eigenvalues parallel to the real axis in the negative imaginary domain, they are the so-called *indifferent states*. Indifferent states only appear if the real part of the energy is large enough, meaning that the CAP is only a small perturbation and the effect of the finite grid is dominant. (4) Finally, the *resonance states*, for which one is looking for, are framed by the real axis, the rotated spectral string (the string states), and the indifferent states. As an illustration of the 1D model results mentioned above by a molecular example, in the case of $(H_2)_2$ the complex eigenvalues of the CAP-modified Hamiltonian form a pattern that is very similar to the pattern in Figures 1 and 2 of ref 9, and this is repeated for each

DOI: 10.1021/acs.jctc.9b00314
J. Chem. Theory Comput. 2019, 15, 4156−4169

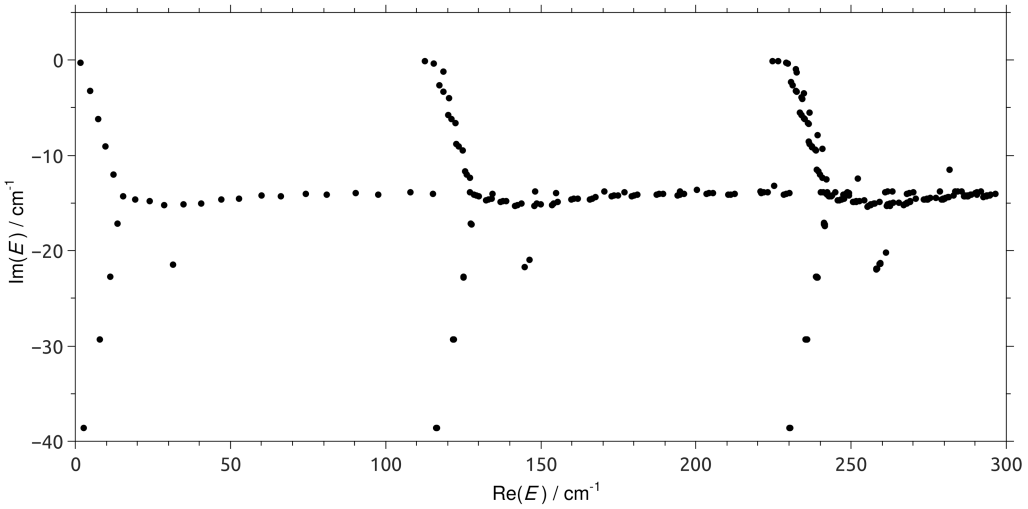

Figure 1. Complex energy eigenvalue pattern of the CAP-modified Hamiltonian $\hat{H}(\eta)$ for $J = 2$ total angular momentum, corresponding to the first three dissociation channels of $(H_2)_2$, where the zero of the horizontal axis marks the first dissociation limit.

dissociation channel, as shown here in Figure 1 for the case of $J = 2$ total angular momentum. Note that the "line" of indifferent states appears only if one computes energies well above the dissociation limit.

The idea to improve the TC method and cure its shortcomings involves the inclusion of the eigenvectors corresponding to the resonance states and *all* string states in the chosen $\{|\phi_k\rangle\}$ basis. With some care, one can select these two types of basis functions by their eigenvalues. Then one solves the eigenvalue equation of the unperturbed Hamiltonian built in this basis, as described in the original TC method. Finally, we propose to identify which complex eigenvalues belong to resonance states based on the fact that resonances are expected to be stable. This means that if one carries out the procedure for slightly different η_{guide} values, for resonance states the variation of the complex energy will be much smaller than for the scattering states. Thus, the computed energies form well-defined clusters which can be identified by carefully chosen clustering algorithms. Let us provide a step-by-step algorithm corresponding to the implementation of what we call the extended TC (ETC) method:

- Perform a bound-state computation. In the subsequent resonance computations, we will use the bound-state and the scattering-state eigenvectors, the latter corresponding to energies above the dissociation limit, obtained with the bound-state-type computation. The number of states to be computed is defined by the energy range to be covered.
- Repeat the following steps for N_η different η_{guide} values, varying them in a predefined small interval:
  (1) Choose a CAP and perform a CAP computation for a given $\eta = \eta_{guide}$ value, solving the eigenvalue equation $\hat{H}(\eta_{guide})|\phi_k\rangle = E_k|\phi_k\rangle$.
  (2) Carefully select the $\{|\phi_k\rangle\}$ basis functions based on the real and imaginary parts of the complex eigenvalues.
  (3) Renormalize the basis functions so that $\langle\phi_k^*|\phi_k\rangle = 1$ and create the complex Hamiltonian matrix $H_{kl} = \langle\phi_k^*|H|\phi_l\rangle$.
  (4) Solve the eigenvalue equation of **H**. This step usually can be done with a direct diagonalization technique, $\mathbf{H}\mathbf{c}_i = E_i\mathbf{c}_i$.
- Collect the E_i complex eigenvalues of **H** corresponding to each η_{guide} value.
- Based on carefully chosen clustering criteria, group the complex eigenvalues into clusters, based principally on their position in the complex plane. Set a threshold for the minimum number of points that defines a cluster, N_{clust}. The recommendation is $N_{clust} \approx 0.5 \times N_\eta$. We recommend the DBSCAN clustering technique,[27] details are given in section 4.2.2.
- To identify the resonances, assign appraisal scores between 0 and 1 for each cluster, based on the variation of the complex energy and the cluster's distance from the line of the rotated spectral string. The appraisal score of the ith cluster corresponding to the variation of energy is $p(i)$, while the slope score $p_s(i)$ describes the cluster's deflection from the rotated spectral string. For the computation of these scores, see section 4.2.2.

The adjustable parameters characterizing the ETC algorithm, for which careful choices are needed, are as follows: (1) The functional form of the CAP. How to choose appropriate CAPs has been discussed in the literature.[28] (2) The coordinate range where the CAP is turned on. The ETC method is as sensitive to these parameters as the original CAP technique. (3) The η_{guide} range. The η_{guide} parameter affects the imaginary energy of the indifferent states and the number of string states. If η_{guide} is too small, one cannot obtain resonances whose imaginary energy is a large negative value, because its wave function will be among the indifferent states in this case. The η_{guide} values used are usually larger than the η values corresponding to cusps. (4) The choice of the $\{|\phi_k\rangle\}$ basis. This step is one of the critical points of the ETC algorithm but it can mostly be performed automatically (see section 4.2.2). (5) The parameters of the clustering algorithm. (6) The parameters of the procedure used to assign appraisal scores to the clusters. The procedure and the clustering parameters form another sensitive part of the ETC algorithm and can obviously depend on the system under study. Details about assigning appraisal scores to the clusters is given in section 4.2.2, here it is only noted that we found that this step can also be made more or less automatic.

For a secure determination of rovibrational resonances one should compare the results of independent computations, i.e., those obtained with different η_{guide} ranges or different CAP

DOI: 10.1021/acs.jctc.9b00314
J. Chem. Theory Comput. 2019, 15, 4156−4169

functions. Since the computations following the usually expensive bound-state computation are inexpensive, due to the small size of **H**, the extra computations do not increase the overall cost of the determination of rovibrational resonances via the ETC method.

3. TEST SYSTEMS

3.1. Ar·NO$^+$. Weakly bound Rg·AB-type complexes (where Rg is a rare-gas atom and AB is a strongly bound diatomic), like Ar·NO$^+$, are ideal systems to study vdW interactions. The stretching vibration of the AB unit is adiabatically separated from the other vibrational degrees of freedom and its fundamental frequency is greater than the first dissociation limit of the complex, which leads to a special energy-level structure of the resonance states. In a previous study on Ar·NO$^+$,[7] the stabilization method has been utilized to find a large number of Feshbach resonances, related to the NO$^+$ stretching overtones, far beyond the first dissociation limit. In the same publication, low-lying resonances, near the first dissociation limit, have been determined with GENIUSH-CAP, a scattering technique, and the stabilization method.

3.2. $(H_2)_2$. $(H_2)_2$ has a special rovibrational energy-level structure, as only the ground state of the intermonomer stretch is bound, and beyond the few bound rovibrational states there is a large number of shape and Feshbach-type rovibrational resonances. The states, for example, where both H_2 molecules are in their rovibrational ground state, and the relative angular momentum (represented by the L diatom quantum number, *vide infra*) is high enough to create a centrifugal barrier allowing the energy to become greater than the dissociation limit, are shape resonances. As to Feshbach resonances, the indistinguishable H_2 molecules are in a rovibrational excited state. As the coupling between the monomer motions and the dissociation coordinate is extremely weak, Feshbach resonances may have a substantial lifetime. The total number of bound and resonance states in a given energy range can be derived for $(H_2)_2$ from angular momentum addition rules, similar to the case of H_2He^+.[29] Since in section 5 the more complex rovibrational resonances of $(H_2)_2$ will be discussed in much more detail than those of Ar·NO$^+$, in what follows we provide a somewhat more elaborate discussion of the states of $(H_2)_2$ to facilitate the appreciation of the computed results. Those familiar with the spectroscopy of $(H_2)_2$ may want to skip the rest of this section.

There exists a significant number of experimental studies[15−20,30,31] which analyzed the high-resolution spectra of $(H_2)_2$. Most quantum-chemical studies[18,32−35] available on the nuclear motions of $(H_2)_2$ have focused on the dimer's few bound states. For example, McKellar and Schaefer[18] computed the $(H_2)_2$ transition frequencies and binding energies relevant in the $S_0(0)$ and $S_0(1)$ transitions. The literature on resonance state computations is considerably smaller, only a few resonances have been determined, using scattering techniques.[33,34]

One can approximate the rotational−vibrational wave functions of $(H_2)_2$ as the product of three diatomic wave functions: those of the two H_2 monomers and that of the "diatom" formed by the centers of mass (COMs) of the two monomers.[36,37] The vibrational and rotational quantum numbers corresponding to the first and second monomers are (v_1, j_1) and (v_2, j_2), respectively, while those of the diatom are denoted as (n, L). To further simplify the model, let us approximate the hydrogen dimer as two interacting rigid H_2 molecules (RM, the bond lengths are frozen), both in their vibrational ground state. The rovibrational wave function can then be written as

$$\Psi_{rv}^{RM} = |j_1 j_2 \pm\rangle |n\rangle |L\rangle \tag{5}$$

where $|n\rangle$ and $|L\rangle$ are the vibrational and rotational wave functions of the diatom, respectively, and

$$|j_1 j_2 \pm\rangle = \frac{1}{\sqrt{2(1 \pm \delta_{j_1 j_2}\delta_{m_1 m_2})}}[Y_{j_1,m_1}(\theta_1, \phi_1)Y_{j_2,m_2}(\theta_2, \phi_2) \pm Y_{j_2,m_2}(\theta_1, \phi_1)Y_{j_1,m_1}(\theta_2, \phi_2)] \tag{6}$$

The rotational wave function of one of the indistinguishable H_2 molecules is $Y_{j,m}(\theta,\phi)$, where $Y_{j,m}(\theta,\phi)$ are the usual spherical-harmonic functions. The total angular momentum is the sum of the angular momenta of the two rigid H_2 molecules and that of the diatom.[36] Coupling the H_2 angular momenta gives $\boldsymbol{J}_1 + \boldsymbol{J}_2 = \boldsymbol{J}_{12}$, while the total angular momentum is the sum of $\boldsymbol{J}_{12}$ and the diatom's angular momentum, $\boldsymbol{L}$, $\boldsymbol{J} = \boldsymbol{J}_{12} + \boldsymbol{L}$. In this study the quantum states are labeled with following five quantum numbers: (j_1, j_2, j_{12}, L, J). This can be derived the following way. There are seven internal degrees of freedom if the H−H bond lengths are fixed. Coupling the H_2 angular momenta, one obtains from the (j_1, j_2, m_1, m_2) quantum numbers $(j_1, j_2, j_{12}, m_{12})$. Adding the diatom angular momentum (denoted by the L and m_L quantum numbers) to this, one obtains $(j_1, j_2, j_{12}, L, J, m_J)$. The seventh descriptor is the intermonomer stretch quantum number, n, which we omit, because it is always assumed to be 0. In the absence of external fields, m_J does not affect the energy; thus, we do not include it in the final label. This way we are left with five quantum numbers. A given state is called symmetric with respect to the exchange of H_2 monomers if $|j_1 j_2+\rangle$ is combined with even L or $|j_1 j_2-\rangle$ is combined with odd L. Antisymmmetric states are characterized by $|j_1 j_2+\rangle$ and odd L or $|j_1 j_2-\rangle$ and even L.

In general, the quantum states of the H_2 dimer can be labeled with the irreducible representations (irreps) of the G_{16} molecular symmetry (MS) group. Bunker and Jensen[36,37] gave a detailed analysis about the determination of symmetry labels and the nuclear spin statistical weights corresponding to each irrep of G_{16}. The total wave function (product of the spin and the spatial parts) of $(H_2)_2$ must be symmetric with respect to the permutation of the monomers. It is important to distinguish the two nuclear spin isomers of the monomeric units when discussing the symmetry properties of the dimer. The *para*-H_2 (p-H_2) molecules have zero nuclear spin and even rotational quantum number. The spin wave function of $(p\text{-}H_2)_2$ is symmetric; thus, the spatial wave function must be also symmetric. *ortho*-H_2 (o-H_2) molecules have odd rotational quantum numbers. The spin wave function of $(o\text{-}H_2)_2$ can be either symmetric or antisymmetric, and these must be combined with symmetric and antisymmetric spatial wave functions, respectively. Application of such rules leads to nuclear spin statistical weights for the H_2 dimer. The spin statistical weight is zero if the symmetry of the spatial wave function is A_2^- or B_2^+. Therefore, these states do not exist in nature, though they do appear in our spin-free nuclear-motion computations.

The depth of the potential well of $(H_2)_2$ is only about 39 cm^{-1},[38] while the rotational constant of the H_2 molecule is about 60 cm^{-1}. This means that even in the $j_1 = 0, j_2 = 1$ state the energy of the dimer is greater than D_e. The H_2 dimer has multiple dissociation channels, corresponding to different (j_1, j_2, j_{12}, L, J) values, where these quantum numbers characterize the

DOI: 10.1021/acs.jctc.9b00314
J. Chem. Theory Comput. 2019, 15, 4156−4169

dissociation products. Note that the dissociation energy depends only on j_1 and j_2. Bound as well as resonance states of $(H_2)_2$ can be found in the energy region close to each dissociation channel. Only those states can be bound where the intermonomer stretch is in the ground state ($n = 0$).[36] The $L = 0$ and 1 states have an energy lower than the corresponding dissociation limit, while states with $L \geq 2$ usually have higher energy. Coupling of $\boldsymbol{J}_{12}$ with $\boldsymbol{L}$, leading to $\boldsymbol{J}$, and the parity of $|j_1 j_2 \pm\rangle$ causes a smaller splitting in the eigenenergies than the contribution of the dimers' end-to-end rotation, described by L.

Bound states exist above the first dissociation limit of $(H_2)_2$ due to symmetry. Assuming that symmetry and J are conserved during dissociation, a state will be bound if it has lower energy than the dissociation limit corresponding to j_1 and j_2 and there is no accessible lower-lying dissociation channel with suitable symmetry and J. Those states whose energy is lower than the corresponding dissociation limit but there is an accessible lower-lying dissociation channel are called negative binding energy resonances. In practice, these states are very similar to bound states and have long lifetimes.

4. COMPUTATIONAL DETAILS

To compute the bound states of the complexes Ar·NO$^+$ and $(H_2)_2$, we used the in-house variational nuclear-motion code GENIUSH.[24,25] GENIUSH employs an iterative Lanczos diagonalization to obtain the eigenvalues. Rovibrational resonances were computed with GENIUSH-CAP[21] and the ETC code developed during this study. In both the GENIUSH-CAP and the ETC methods, the eigenvectors of the original Hamiltonian obtained with GENIUSH are used as a basis to obtain the matrix representation of the CAP-perturbed Hamiltonian. The complex eigenvalues of the matrix are computed via direct diagonalization, using the "LaEigSolve" function from the Lapack++ package.[41] Characteristics of the semi-automated ETC method are discussed in detail below only for $(H_2)_2$.

The most time-consuming part of the computation of the resonances is the GENIUSH run, which can take a couple of days. ETC computations are considerably less expensive, they can be done in half an hour. The size of the file containing the GENIUSH eigenvectors is a few gigabyte. ETC requires only a small amount of memory.

4.1. Ar·NO$^+$. Only a brief description is provided here; some of the details can be found in section 4.2.

4.1.1. GENIUSH and GENIUSH-CAP Computations. The $J = 0$ low-lying vibrational resonances of the Ar·NO$^+$ complex[7] form our first test of the ETC method. The computational parameters of the GENIUSH run are very similar to those of the original study of Ar·NO$^+$.[7] We used the three-dimensional (3D) HSLH potential energy surface (PES)[42] describing the ground electronic state of Ar·NO$^+$. The structure was represented by Jacobi coordinates: r is the N−O bond length, R is the distance of the Ar atom and the COM of the NO$^+$ unit, while θ is the angle of the NO vector and the vector connecting the COM of NO$^+$ and the Ar atom. The GENIUSH code employs a DVR[22,43] of the vibrational Hamiltonian. The basis functions are direct products of DVR functions,[23,39,40] with each term in the product being a function of a single degree of freedom. Table 1 shows the type, the number, and the range of the basis functions employed during the bound-state and the resonance computations. We performed two GENIUSH computations, using 15 and 20 grid points on the r coordinate, as they result in somewhat different resonances. This sensitivity to the choice of the DVR functions will be discussed later. We used the following masses: $m(^{40}\mathrm{Ar}) = 39.962\,383$ u, $m(^{14}\mathrm{N}) = 14.003\,074$ u, and $m(^{16}\mathrm{O}) = 15.994\,915$ u.

Table 1. Basis Functions Employed in Bound-State and Resonance Rovibrational Computations on Ar·NO$^+$ and $(H_2)_2$

molecule	coordinate	range/(bohr or °)	basis type	no. of basis functions
Ar·NO$^+$	r	[1.68, 2.64]	Laguerre-DVR	15 and 20
	R	[4.0, 50.0]	Laguerre-DVR	150
	θ	(0, 180)	Legendre-DVR	100
$(H_2)_2$	R for bound states, $J = 0$	[3.0, 25.0]	Laguerre-DVR[a]	16
	R for bound states, $J \neq 0$	[3.0, 25.0]	Fourier-DVR[b]	25
	R for resonances	[3.0, 60.0]	Fourier-DVR	45−61
	θ_1, θ_2	(0, 180)	Legendre-DVR[c]	40−250[d]
	ϕ	[0, 360)	Fourier-DVR	7−11

[a]See ref 39. [b]See ref 40. [c]See ref 23. [d]See text.

The GENIUSH eigenvectors obtained this way form the basis in the GENIUSH-CAP computations. The range chosen for the η parameter is $10^{-8} - 10^{-1}$, each GENIUSH-CAP trajectory covering 2−3 orders of magnitude and 500 η values. We apply the fifth-order polynomial CAP function of ref 28. The R coordinate, where the CAP is switched on changes from 15 to 45 bohr, in steps of 5 bohr. This is done because the wave function of some resonances is localized far from the interaction region of the PES. Those features are recognized as resonances where multiple trajectories, corresponding to different CAP start values, have a cusp.

4.1.2. ETC computations. We employ the fifth-order polynomial CAP function of ref 28, and perform separate ETC computations for each CAP turn-on value, similar to the case of the GENIUSH-CAP computations. The range chosen for η_{guide} is $[1.0 \times 10^{-4}, 1.1 \times 10^{-4}]$, with $N_\eta = 11$ different η_{guide} values. After solving the eigenvalue equation of $\hat{H} - i\eta_{\mathrm{guide}}\hat{W}$, the pattern of complex eigenvalues was found to be as follows: there are many resonances and there are multiple lines of string states and diverging states in the energy region of interest. The ETC basis functions are selected based on the following energy criteria: 885 cm^{-1} < Re(E) < 910 cm^{-1} (the first dissociation energy being $D_0 \approx 887$ cm^{-1}) and $\mathrm{Im}_{\mathrm{min}} < \mathrm{Im}(E) < 0$ cm^{-1}. $\mathrm{Im}_{\mathrm{min}}$, the boundary between the string states and the diverging states was clearly visible, and was set manually. The ETC basis functions are divided into two groups by the imaginary part of the energy, one from −0.1 cm^{-1} to 0.0 cm^{-1} and the other from $\mathrm{Im}_{\mathrm{min}}$ to −0.1 cm^{-1}. After solving the eigenvalue equation of the unperturbed Hamiltonian matrix built in this basis, we collect the complex eigenvalues corresponding to the two groups of basis functions and the 11 η_{guide} values. Then we plot the eigenvalues in the complex plane and determine the clusters with the DBSCAN ("density-based spatial clustering of applications with noise") technique (see section 4.2.2 for details).[27] The minimum number of points in a cluster is set to $N_{\mathrm{clust}} = 5$; however, in most cases, there are 11 points in a cluster due to the $N_\eta = 11$ choice. The line of the string states is not determined, only the $p(i)$ appraisal score is computed. Note that the above procedure is for a single CAP turn-on value. The clusters whose appraisal scores are $p(i) > 0.8$ (eq 15, *vide infra*) and which appear for at least two CAP starting values are very likely

DOI: 10.1021/acs.jctc.9b00314
J. Chem. Theory Comput. 2019, 15, 4156−4169

resonances. We compute the centroid of each cluster and make a 2D histogram binning of these points to decide which ones appear for more CAP starting values.

4.2. $(H_2)_2$. As this is the first paper on the application of the ETC method, we describe in detail the practical implementation of the method for $(H_2)_2$.

4.2.1. GENIUSH and GENIUSH-CAP Computations. During the nuclear-motion computations for $(H_2)_2$ we only treat four internal degrees of freedom out of the six possible, the H_2 bond lengths are kept fixed at their expectation value in the vibrational ground state: $r_{1,0} = r_{2,0} = r_0 = 1.448\,736$ bohr.[44] The mass of the hydrogen atom is set to $m(^1H) = 1.007\,825$ u. In the internal coordinate system chosen for the GENIUSH and GENIUSH-CAP computations R is the distance of the two centers of mass (COM), θ_1 and θ_2 are the angles between the H−H bonds and the COM−COM line, and ϕ is a torsion angle. We employ a 6D PES of $(H_2)_2$ developed by Hinde.[38]

Using the GENIUSH code, we compute the lowest few hundred eigenvalues of the Hamiltonian via an iterative Lanczos diagonalization; therefore, we obtain a few bound states, some resonance states, and a large number of scattering states in the energy range covered. Bound states have well-defined real energies, it is straightforward to obtain converged results for them. Resonances are characterized by energy uncertainties and scattering states have continuum energy; therefore, their calculated energy will depend on the actual parameters of the computation (for example, the size of the basis and the coordinate ranges).

Because the GENIUSH-CAP code utilizes the eigenvalues and eigenvectors computed by the GENIUSH code, bound states are obtained as "byproducts" of the resonance computations. Nonetheless, we perform separate GENIUSH runs for obtaining just the bound states, as bound-state computations require smaller basis sets and a smaller R range than resonance computations to achieve convergence.

For $(H_2)_2$, we have to introduce two corrections to the rovibrational energies obtained by GENIUSH. The corrections concern both the bound and the resonance states. The first correction is related to how we set the angular (θ_1 and θ_2) basis. Convergence with respect to the θ_1 and θ_2 bases requires many functions, which makes the diagonalization of the Hamiltonian slow. Therefore, we make the resonance computations with 40 functions on both the θ_1 and θ_2 coordinates, and add a correction term for each bound and resonance state, thus mimicking the computations utilizing a much larger number of basis functions (250, 120, 120, and 100 for the $J = 0$, 1, 2, and 3 cases, respectively). We obtain the related energy correction the following way: (a) perform two 3D computations ($R = 6.35$ bohr, fixed at equilibrium) with 40 functions ($E^{3D;40}_{j_1,j_2,j_{12},L,J}$ energies) and the larger basis ($E^{3D;large}_{j_1,j_2,j_{12},L,J}$ energies); and (b) the $E^{corr}_{j_1,j_2,j_{12},L,J}$ correction term is the energy difference of these two computations,

$$E^{corr}_{j_1,j_2,j_{12},L,J} = E^{3D;large}_{j_1,j_2,j_{12},L,J} - E^{3D;40}_{j_1,j_2,j_{12},L,J} \tag{7}$$

which is added to the (j_1, j_2, j_{12}, L, J) energy in the 4D computation. This correction technique is validated by comparing the correction terms to the energy difference of 4D energies obtained with 40 functions and a larger basis.

The second correction is due to fixing the H−H bond length to r_0. If we calculate the rotational energies of the hydrogen molecule in the rigid-rotor model using r_0, we observe significant differences from the real energies.[45] However, the binding energies of $(H_2)_2$ agree reasonably well with the literature values.[18] The $E^{bind}_{j_1,j_2,j_{12},L,J}$ binding energy of a given state is the energy difference from $E^{diss}_{j_1,j_2}$, the dissociation channel's energy,

$$E^{diss}_{j_1,j_2} = B_{r_0}(j_1(j_1+1) + j_2(j_2+1)) \tag{8}$$

where $B_{r_0} = 56.919$ cm^{-1} is the rotational constant obtained from r_0. Then,

$$E^{bind}_{j_1,j_2,j_{12},L,J} = E^{raw}_{j_1,j_2,j_{12},L,J} - E^{diss}_{j_1,j_2} \tag{9}$$

where $E^{raw}_{j_1,j_2,j_{12},L,J}$ is the result of the GENIUSH computations. We determine the $E_{j_1,j_2,j_{12},L,J}$ final $(H_2)_2$ energies as

$$E_{j_1,j_2,j_{12},L,J} = E_{j_1} + E_{j_2} + E^{raw}_{j_1,j_2,j_{12},L,J} - E^{diss}_{j_1,j_2} + E^{corr}_{j_1,j_2,j_{12},L,J} \tag{10}$$

where E_j is the rotational energy of H_2 (calculated with the help of eq 2 and the constants from Table II of ref 45) and $E^{corr}_{j_1,j_2,j_{12},L,J}$ is the theta basis correction term.

As to the resonance computations, the basis parameters of the GENIUSH runs are presented in Table 1. If the eigenvectors coming from the bound-state computation are used for subsequent resonance computations, the R coordinate range has to be chosen rather wide as the resonance wave functions might remain significant far away from the interaction region. In GENIUSH-CAP, we use three polynomial CAP functions:[28] second-, third-, and fifth-order polynomials, called W2CAP, W3CAP, and W5CAP, respectively. The CAP is turned on between 15.0 bohr and the end of the grid. The η range is 10^{-7}−10^{-4}, each inexpensive trajectory computation covering usually 2−3 orders of magnitude and 300−500 η values.

During this study, we utilize the symmetry of the eigenstates of the $(H_2)_2$ complex. Symmetry labels of the states can be obtained the following way. Calculate the energies and wave functions of a reduced-dimensional (3D) model with $R = 6.35$ bohr (fixed at equilibrium), while the θ_1, θ_2, ϕ basis is the same as in the 4D calculation. We can then straightforwardly assign the (j_1, j_2, j_{12}, L, J) quantum numbers and the symmetry labels to these states based on just energy criteria: for a given j_1 and j_2, the energy is increasing with L, while for a given j_1, j_2, and L group, the energy is increasing with the j_{12} quantum number. Then we calculate the overlap of each 3D and 4D wave function by fixing R at given values in the 4D case and then integrating along the R coordinate. If a 4D state has a given symmetry label, it has nonzero overlap only with those 3D states that have the same symmetry label; therefore, the symmetry of 4D wave functions can be assigned based on their overlaps with 3D wave functions. If $j_1 \neq j_2$, and both are even or odd, both the + or − combinations are allowed in $|j_1 j_2 \pm\rangle$.[36] However, there is no straightforward connection between the +/− combination and the energy of the 3D states. Thus, the +/− combination is determined by comparison with literature data and overlaps with 3D states of known symmetry labels.

4.2.2. ETC Computations. We use a second-order CAP function,[28] turned on at 15.0 bohr, as in the GENIUSH-CAP computations. We perform computations for two groups of η_{guide} values, with $N_\eta = 11$ points evenly distributed in the $[5 \times 10^{-5}, 6 \times 10^{-5}]$ and $[1 \times 10^{-4}, 1.1 \times 10^{-4}]$ intervals. The basis functions (some eigenvectors of the CAP-perturbed Hamiltonian) for the ETC method are selected based on the real and imaginary parts of the energy: $Re_{min} < Re(E) < Re_{max}$ and $Im_{min} < Im(E) < 0$ cm^{-1}. The limits for the real part are set manually for

DOI: 10.1021/acs.jctc.9b00314
J. Chem. Theory Comput. 2019, 15, 4156−4169

each dissociation channel. $\mathrm{Im}_{\min}$ is set to be "just above" the line of indifferent states, and it is computed automatically for each η_{guide} as $\mathrm{Im}_{\min} = 0.95 \cdot \mathrm{Median}(\mathrm{Im}(E))$, because we found that it is advantageous to include as many string states in the basis as possible. We then renormalize the basis functions and solve the eigenvalue equation of the unperturbed Hamiltonian built in this basis.

After collecting the complex eigenvalues corresponding to the 11 η_{guide} values in the two η_{guide} groups different in their intervals, we locate the resonances the following way. The eigenvalues are plotted in the complex plane, the real and imaginary parts interpreted as x and y coordinates. First, we need to determine the line of the rotated spectral string. Most of the computed points are on this line and the resonances are off of this line. Therefore, we employ a robust linear fitting method to determine the parameters of the spectral string line. For this we employ two methods, the Theil−Sen estimator[46,47] and an iterative weighted linear fit method that reduces the weight of the outlier points and increases the weight of points close to the line. Both methods resulted in similar fitting parameters m and b ($y = mx + b$).

Next, we group the points into clusters to identify the resonances. The points in each cluster belong to a given eigenvalue of the unperturbed Hamiltonian's matrix obtained with the different $\eta = \eta_{\mathrm{guide}}$ values. Resonance eigenvalues are expected to be stable, i.e., the variation of the points in their cluster should be small. In contrast, the energy of other (string and scattering) states changes considerably more with the change of η_{guide}. (Note that energy stabilization also characterizes the traditional CAP technique, the points of the trajectory are denser in the region of the cusp.) Before clustering, we discard the points on the real axis corresponding to negative binding energy states, and points on the real axis at large energies, because these are indifferent states. We only aim to identify the points corresponding to string states and resonances.

To group the points into clusters, we have to define the d_{ij} distance of the ith and jth points, which can depend on the system under study. In the case of $(H_2)_2$,

$$d_{ij} = \frac{\sqrt{(x_i - x_j)^2 + (y_i - y_j)^2}}{|x_i - x_0|} \tag{11}$$

where $x_0 = -b/m$ is the intercept on the x (real) axis. One can also use the corresponding dissociation energy $E^{\mathrm{diss}}_{j_1 j_2}$ instead of x_0. Scaling with $|x_i - x_0|$ is necessary because the variation of points in a cluster is smaller close to the dissociation energy than at higher energies. We have tried two clustering algorithms. The first one, called "rectangle clustering", can be described as follows. The size of the rectangle which defines the cluster is Δx and Δy along the x and y coordinates, respectively. The distance of the points along the x axis must be less than Δx, and the distance along the y axis must be less than Δy. In the case of $(H_2)_2$, for the ith point the jth point is *close*, i.e., in the same cluster, if

$$|x_i - x_j|/|x_i - x_0| < \Delta x \tag{12}$$

and

$$|y_i - y_j|/|x_i - x_0| < \Delta y \tag{13}$$

We set Δx and Δy such that we find the largest number of clusters in a way that there are not (much) more points in a cluster than N_η. The second clustering algorithm tried is the DBSCAN technique,[27] whereby clusters are determined by the density of points and the overall size of the cluster is not specified, contrary to the rectangle clustering. A core point of a cluster must have a set number of neighboring points (minPts) in a given ϵ radius, not counting itself. Points on the edge of a cluster do not have minPts neighbors themselves, but they are neighbors of a core point. Noise points are solitary, lying away from the core points. When determining the d_{ij} distance of the ith and jth points, the Euclidean distance was divided by $|x_i - x_0|$. The value of 2 was found to be adequate for minPts because clusters are usually string-like (in fact, pieces of a trajectory), and the ϵ value can be chosen to cluster as many points as possible without merging clusters. The minimum number of points required to form a cluster is set to $N_{\mathrm{clust}} = 5$ in both clustering techniques. Even though the two clustering techniques result in similar resonances, we prefer DBSCAN as it is more capable of following the natural shapes of clusters.

Then, we determine the appraisal score, a value between 0 and 1, for each cluster. Clusters which do not lie on the line of the rotated spectral string and whose variance is small are likely to be resonances. Let l_i be the length of the ith cluster divided by the n_{clust} number of its points. To obtain the length, we add the distance of the consecutive j and k points (corresponding to increasing η_{guide}) along the cluster:

$$l_i = \frac{\sum d_{jk}}{n_{\mathrm{clust}}} \tag{14}$$

Note that this is not applicable for merged clusters; therefore, we do not assign appraisal scores to clusters where n_{clust} is much larger than N_η. The $p(i)$ total appraisal score corresponding to the variance of a cluster is

$$p(i) = \frac{l_i - \max(l)}{\min(l) - \max(l)} \tag{15}$$

where $\min(l)$ and $\max(l)$ are the minimum and maximum of the l_i values, respectively. The most extended cluster gets an appraisal score of 0, while the most compact one gets 1.

It is also helpful to determine which clusters lie on the line of the rotated spectral string; therefore, we assigned slope scores for the clusters based on their deflection from the rotated spectral string. We fit a line through the $(x_0,0)$ point and the $(\langle x\rangle_i,\langle y\rangle_i)$ centroid of the cluster, where $\langle x\rangle_i$ means the expectation value in the ith cluster. The slope of the line is

$$m_i = \frac{\langle y\rangle_i}{\langle x\rangle_i - x_0} \tag{16}$$

The $p_s(i)$ slope score is 0 for the rotated spectral string and clusters below it, and 1 for the most deflected cluster:

$$p_s(i) = \begin{cases} \dfrac{m_i - m}{\max(m) - m} & \text{if } m_i \geq m \\ 0 & \text{otherwise} \end{cases} \tag{17}$$

where $\max(m)$ is the maximum of the m_i values.

The clusters whose slope score is $p_s(i) < 0.3$ are regarded as part of the rotated spectral string. There can be clusters with $p_s(i) \geq 0.3$ that are not resonances. The following examples can be provided: (a) if the cluster belongs to the rotated spectral string but its deviation from the line is large, or (b) if the cluster corresponds to an indifferent state, but was chosen to be part of the basis set by mistake. Resonances can be distinguished from

DOI: 10.1021/acs.jctc.9b00314
J. Chem. Theory Comput. 2019, 15, 4156−4169

these "false positives" by the appraisal score. The "false positive" clusters are expected to be extended, while resonances should form a compact cluster. According to our experience, if a cluster (a) appears in the case of both groups of η_{guide} values, $[5 \times 10^{-5}, 6 \times 10^{-5}]$ and $[1.0 \times 10^{-4}, 1.1 \times 10^{-4}]$, (b) has $p_s(i) \geq 0.3$, and (c) has $p(i) \geq 0.6$, it is very likely to be a resonance. $p(i) \geq 0.8$ means sharp resonances, while less sharp ones have $0.6 \leq p(i) < 0.8$. If $p(i) < 0.6$, the cluster is a "false positive", in the sense that it is deflected from the line, just like resonances are. Note that the appraisal and slope score limits given are empirical, they can vary with the clustering method and can be different for different systems.

5. RESULTS AND DISCUSSION

5.1. Rovibrational Resonances of Ar·NO$^+$. The results obtained with the current GENIUSH-CAP and ETC methods are shown in Table 2. We present only those computed low-lying vibrational resonances of Ar·NO$^+$ whose lifetime is greater than 15 ps and whose energy is less than D_0 + 20 cm^{-1}. Those ETC clusters that have good appraisal scores and appear for at least two CAP starting values are accepted as resonances. In Table 2 we present results obtained with both 15 and 20 GENIUSH DVR basis functions on the r coordinate, the computational results are seemingly somewhat sensitive to the choice of the basis. In the resonance computations we use the GENIUSH eigenvalues and eigenvectors corresponding to bound states as well as to states above the dissociation limit. The latter scattering eigenvectors vary with the GENIUSH DVR basis even if the bound states are converged. Therefore, the basis in the ETC method will become basis dependent, as well. Some resonances can be found only with either 15 or 20 basis functions. If a resonance is present in both computations, the agreement between the GENIUSH-CAP and the ETC results is better than the agreement of the GENIUSH-CAP results obtained with 15 and 20 r basis functions. Comparing the GENIUSH-CAP and the ETC results, we find that the real energies and the lifetimes agree well. There is only one resonance which is missing in the case of the ETC method, and there are only a few false positives, where no cusps are found on the GENIUSH-CAP trajectories. The false positive resonances are all short-lived ones; thus, they are not reported in Table 2.

Table 2. Low-Lying Vibrational Resonances of Ar·NO$^+$ Obtained with the GENIUSH-CAP and the ETC Methods[a]

15 basis functions on r				20 basis functions on r			
GENIUSH-CAP		ETC		GENIUSH-CAP		ETC	
$E - D_0$	lifetime	$E - D_0$	lifetime	$E - D_0$	lifetime	$E - D_0$	lifetime
0.5	69	0.4	83	0.5	43	0.5	40
0.7	65	0.6	70				
				1.0	1758	1.0	1770
1.7	107	1.7	161	1.7	372	1.7	531
2.6	>2655	2.6	>2655	2.6	1252	2.6	1062
2.8	18	2.8	19	2.9	29	2.9	31
				3.0	63	–	–
4.6	44	4.6	50				
				5.0	79	5.0	80
8.6	56	8.6	52	8.7	87	8.7	86
9.5	15	9.4	14	9.5	15	9.5	15
10.1	92	10.1	103	10.1	88	10.1	100
10.7	51	10.7	52	10.8	65	10.8	66
11.1	37	11.1	34				
				11.6	65	11.6	70
				13.3	33	13.3	33
16.4	40	16.4	41	16.5	57	16.5	58
17.6	49	17.6	49				
				18.2	35	18.2	35
18.8	60	18.8	59	18.8	56	18.8	56
19.5	15	19.5	15				

[a]Energies are in cm^{-1}, lifetimes in ps. The real part of the energy is measured from D_0 = 887 cm^{-1}.

5.2. Bound States and Resonances with Negative Binding Energies of $(H_2)_2$. Tables 3–6 show the bound states and the resonances with negative binding energy of $(H_2)_2$ for J = 0, 1, 2, and 3, respectively. Resonances with negative binding energy have lower energy than $E^{diss}_{j_1,j_2}$ but higher energy than a symmetry-allowed lower-lying dissociation channel; thus, their real energy is very stable, similarly to bound states. The energies presented in Tables 3–6 include the corrections described in the section Computational Details. The last column of the tables show the binding energies obtained by McKellar and Schaefer.[18,35] The agreement between the two sets of results, when a match is possible, is better than 0.2 cm^{-1}. We found two states, $(j_1, j_2, j_{12}, L, J) = (3, 1, 2, 2, 1)$ and $(3, 0, 3, 1, 3)$, which are not listed in ref 18. As another comparison with the literature, we determined transition frequencies for the $S_0(0)$ and $S_0(1)$ transitions and compare them to those computed in ref 18; see Table 7 for the results. The agreement in the transition wavenumbers is better than 0.2 cm^{-1}.

As stated above, there are bound states above the first dissociation limit if there is no accessible dissociation channel with suitable symmetry and J. In some cases even the first state within a given irreducible representation and J has an energy higher than $E^{diss}_{j_1,j_2}$, meaning that there is no bound state with that symmetry. This situation occurs when $L \geq 2$, e.g., $(j_1, j_2, j_{12}, L, J) = (2, 1, 2, 2, 0)$ is an E^- state, $(1, 1, 2, 2, 1)$ is a B_1^+ state, and $(1, 1,$

Table 3. J = 0 Bound States and Resonances with Negative Binding Energies for $(H_2)_2$

state	j_1	j_2	±	j_{12}	L	irrep	E/cm^{-1}	E^{bind}/cm^{-1}	literature E^{bind}/cm^{-1}
bound	0	0	+	0	0	A_1^+	−2.95	−2.95	−2.8495[35]
bound	1	0	±	1	1	E^+	116.72	−1.78	−1.718074[35]
bound	1	1	+	0	0	B_1^+	233.97	−3.02	−2.946408[35]
bound	1	1	−	1	1	A_1^-	235.97	−1.02	−0.885110[35]
bound	2	0	−	2	2	B_2^+	354.16	−0.23	
resonance	2	1	±	1	1	E^+	471.25	−1.63	
resonance	2	2	+	0	0	A_1^+	705.78	−3.01	
bound	2	2	−	1	1	B_1^-	707.70	−1.08	
bound	3	1	−	2	2	A_2^+	823.77	−0.27	−0.14367[18]

DOI: 10.1021/acs.jctc.9b00314
J. Chem. Theory Comput. 2019, 15, 4156–4169

Table 4. $J = 1$ Bound States and Resonances with Negative Binding Energy for $(H_2)_2$

state	j_1	j_2	±	j_{12}	L	irrep	E/cm^{-1}	E^{bind}/cm^{-1}	literature E^{bind}/cm^{-1}
bound	0	0	+	0	1	A_2^-	−1.39	−1.39	−1.2986[35]
bound	1	0	±	1	0	E^-	115.51	−2.98	−2.874909[35]
bound	1	0	±	1	1	E^+	117.28	−1.22	−1.102486[35]
bound	1	1	−	1	0	A_2^+	234.01	−2.98	−2.862182[35]
bound	1	1	+	0	1	B_2^-	234.94	−2.06	−2.009345[35]
bound	1	1	−	1	1	A_1^-	235.40	−1.59	−1.504722[35]
bound	1	1	+	2	1	B_2^-	235.65	−1.34	−1.234314[35]
bound	2	0	−	2	1	B_1^-	352.43	−1.96	−1.79235[18]
resonance	2	0	+	2	1	A_2^-	352.61	−1.78	
resonance	2	1	±	1	0	E^-	469.86	−3.03	
resonance	2	1	±	1	1	E^+	471.25	−1.64	
resonance	2	1	±	2	1	E^+	471.72	−1.17	
resonance	2	2	−	1	0	B_2^+	705.75	−3.04	
resonance	2	2	+	0	1	A_2^-	707.07	−1.72	
resonance	2	2	−	1	1	B_1^-	707.15	−1.64	
resonance	2	2	+	2	1	A_2^-	707.63	−1.16	
resonance	3	1	−	2	1	A_1^-	822.05	−1.99	−1.85607[18]
resonance	3	1	+	2	1	B_2^-	822.07	−1.98	−1.82331[18]
resonance	3	1	+/−	2	2	B_1^+/A_2^+	823.84	−0.21	

Table 5. $J = 2$ Bound States and Resonances with Negative Binding Energy of $(H_2)_2$

state	j_1	j_2	±	j_{12}	L	irrep	E/cm^{-1}	E^{bind}/cm^{-1}	literature E^{bind}/cm^{-1}
bound	1	0	±	1	1	E^+	117.05	−1.45	−1.353384[35]
bound	1	1	+	2	0	B_1^+	233.86	−3.13	−3.015411[35]
bound	1	1	−	1	1	A_1^-	235.61	−1.38	−1.260316[35]
bound	1	1	+	2	1	B_2^-	235.71	−1.28	−1.144977[35]
bound	2	0	−	2	0	B_2^+	351.28	−3.11	
resonance	2	0	+	2	0	A_1^+	351.37	−3.03	
bound	2	0	+	2	1	A_2^-	353.13	−1.26	
bound	2	0	−	2	1	B_1^-	353.14	−1.25	
resonance	2	1	±	2	0	E^-	469.84	−3.05	
resonance	2	1	±	1	1	E^+	470.92	−1.97	
resonance	2	1	±	2	1	E^+	471.38	−1.51	
resonance	2	1	±	3	1	E^+	471.61	−1.28	
resonance	3	0	±	3	1	E^+	703.97	−1.58	−1.46405[18]
resonance	2	2	+	2	0	A_1^+	705.75	−3.03	
resonance	2	2	−	1	1	B_1^-	707.05	−1.74	
resonance	2	2	+	2	1	A_2^-	707.23	−1.56	
resonance	2	2	−	3	1	B_1^-	707.53	−1.25	
resonance	3	1	+	2	0	B_1^+	820.83	−3.21	−3.06778[18]
resonance	3	1	−	2	0	A_2^+	820.85	−3.19	−3.06482[18]
resonance	3	1	+	2	1	B_2^-	822.19	−1.86	−1.61796[18]
resonance	3	1	−	2	1	A_1^-	822.24	−1.81	−1.54103[18]
resonance	3	1	+	3	1	B_2^-	822.84	−1.20	−1.11660[18]
resonance	3	1	−	3	1	A_1^-	822.89	−1.15	−1.08338[18]

1, 2, 2) is a A_2^+ state, the first members of their symmetry, but they are not bound states (thus, these states are shown in the tables reporting resonances). If J is large, the lowest states, when j_1 and j_2 are small, will be resonances, as L must be large. For $J \geq 2$, the even state corresponding to $(j_1, j_2) = (0, 0)$ is a resonance.

An example for a negative binding energy resonance is the $(j_1, j_2, j_{12}, L, J) = (2, 0, 2, 1, 1)$ A_2^- state, where the dissociation channel corresponding to $(0, 0, 0, 1, 1)$ is accessible; thus, it is a resonance state. Negative binding energy resonances have extremely long lifetimes, the real part of the energy computed is very stable, and the imaginary part is very close to zero. We compute the energies of these states with the bound-state code GENIUSH. We discuss these states in this section because their lifetimes cannot be evaluated precisely.

Finally, issues related to the choice of the fixed H_2 bond length must be discussed. To facilitate this discussion, we performed electronic-structure computations for $(H_2)_2$ using the CFOUR[48] code. The level of computation was full configuration interaction (FCI) with the aug-cc-pVQZ basis.[49] The equilibrium bond lengths of the monomers obtained are $r_{e,1}$ = 1.4034 bohr and $r_{e,2}$ = 1.4035 bohr, which result in rotational constants close to B_e = 60.853 cm^{-1}:[50] $B_{r_{e,1}}$ = 60.653 cm^{-1} and $B_{r_{e,2}}$ = 60.648 cm^{-1}. The computed r_g values are close to the bond lengths employed in the GENIUSH computations: $r_{g,1}$ = 1.4497 and $r_{g,2}$ = 1.4486 bohr, resulting in $B_{r_{g,1}}$ = 56.842 cm^{-1} and $B_{r_{g,2}}$ = 56.930 cm^{-1}. To study the effect of fixing the H−H bond lengths, we computed the $J = 0$ bound states with GENIUSH up

DOI: 10.1021/acs.jctc.9b00314
J. Chem. Theory Comput. 2019, 15, 4156−4169

Table 6. $J = 3$ Bound States and Resonances with Negative Binding Energy of $(H_2)_2$

state	j_1	j_2	±	j_{12}	L	irrep	E/cm^{-1}	E^{bind}/cm^{-1}	literature E^{bind}/cm^{-1}
bound	1	1	+	2	1	B_2^-	235.41	−1.58	−1.47971[18]
bound	2	0	−	2	1	B_1^-	352.82	−1.57	
resonance	2	0	+	2	1	A_2^-	352.87	−1.52	
resonance	2	1	±	3	0	E^-	469.81	−3.08	
resonance	2	1	±	2	1	E^+	471.39	−1.50	
resonance	2	1	±	3	1	E^+	471.67	−1.22	
resonance	3	0	±	3	0	E^-	702.54	−3.01	−2.86517[18]
resonance	3	0	±	3	1	E^+	704.32	−1.23	
resonance	2	2	−	3	0	B_2^+	705.74	−3.04	
resonance	2	2	+	2	1	A_2^-	707.01	−1.78	
resonance	2	2	+	4	1	A_2^-	707.38	−1.41	
resonance	2	2	−	3	1	B_1^-	707.39	−1.40	

Table 7. Computed $S_0(0)$ and $S_0(1)$ Transition Wavenumbers of $(H_2)_2$[a]

$(j_1', j_2', j_{12}', L', J')$	→	$(j_1'', j_2'', j_{12}'', L'', J'')$	ΔE_{comp}/cm^{-1}	$\Delta E_{lit.}$/cm^{-1}
		para-H_2−*para*-H_2		
(0, 0, 0, 0, 0)		(0, 2, 2, 1, 1)	355.38	355.4301[18]
		para-H_2−*ortho*-H_2		
(1, 0, 1, 1, 2)		(3, 0, 3, 0, 3)	585.49	585.5202[18]
(1, 0, 1, 0, 1)		(3, 0, 3, 1, 2)	588.45	588.4429[18]
		Symmetric *ortho*-H_2−*ortho*-H_2		
(1, 1, 1, 1, 2)		(1, 3, 2, 0, 2)	585.22	585.2245[18]
(1, 1, 1, 1, 1)		(1, 3, 2, 0, 2)	585.44	585.4689[18]
(1, 1, 0, 0, 0)		(1, 3, 2, 1, 1)	588.08	588.1223[18]
(1, 1, 2, 0, 2)		(1, 3, 2, 1, 1)	588.19	588.1913[18]
(1, 1, 2, 0, 2)		(1, 3, 2, 1, 2)	588.38	588.5064[18]
(1, 1, 2, 0, 2)		(1, 3, 3, 1, 2)	589.03	588.9640[18]
		Antisymmetric *ortho*-H_2−*ortho*-H_2		
(1, 1, 2, 1, 2)		(1, 3, 2, 0, 2)	585.14	585.1122[18]
(1, 1, 2, 1, 1)		(1, 3, 2, 0, 2)	585.21	585.2015[18]
(1, 1, 2, 1, 3)		(1, 3, 2, 0, 2)	585.45	585.4469[18]
(1, 1, 0, 1, 1)		(1, 3, 2, 0, 2)	585.92	585.9765[18]
(1, 1, 1, 0, 1)		(1, 3, 2, 1, 1)	588.06	588.0709[18]
(1, 1, 2, 1, 1)		(1, 3, 2, 2, 0)	588.13	588.1226[18]
(1, 1, 1, 0, 1)		(1, 3, 2, 1, 2)	588.18	588.2762[18]
(1, 1, 1, 0, 1)		(1, 3, 3, 1, 2)	588.84	588.7776[18]
(1, 1, 0, 1, 1)		(1, 3, 2, 2, 0)	588.84	588.8977[18]

[a]The literature (lit.) data correspond to computations and not to experiment.

to $(j_1, j_2) = (2, 2)$ using four different bond lengths: r = 1.438 736, 1.428 736, and 1.418 736 bohr, and the equilibrium bond length of H_2, r_e = 0.741 44 Å[S1] (~1.401 1 bohr). The resulting energies are $\tilde{E}^{r\neq r_0}_{j_1,j_2,j_{12},L,J}$,

$$\tilde{E}^{r\neq r_0}_{j_1,j_2,j_{12},L,J} = E^{\mathrm{raw};r\neq r_0}_{j_1,j_2,j_{12},L,J} + E^{\mathrm{corr}}_{j_1,j_2,j_{12},L,J} \quad (18)$$

i.e., we do not use the real rotational energies of H_2, see eq 10. To determine which r value is the best to reproduce the $E_{j_1,j_2,j_{12},L,J}$ energies obtained with eq 10 and r_0, we plotted

$$\Delta(r) = \sum_i (\tilde{E}^{r\neq r_0}_{j_1,j_2,j_{12},L,J} - E_{j_1,j_2,j_{12},L,J})^2 \quad (19)$$

as a function of bond length in Figure 2. The quadratic function fitted to the points of Figure 2 reveals that the difference is minimal when r = 1.422 6 bohr.

5.3. Resonances of $(H_2)_2$. *5.3.1. GENIUSH-CAP Results.* In Tables 8−10, we present the results of resonance computations

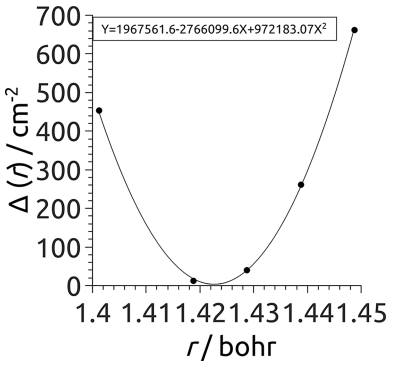

Figure 2. Calculating which H−H bond length (r) one should use in GENIUSH to get the best energies without the bond length correction. $\Delta(r)$ (see eq 19) describes the difference from the energies computed with r_0 and the correction term (see eq 10).

for J = 0, 1 and 2, respectively. The energies listed include the two correction terms discussed in the section on Computational details. We determined the energies and lifetimes of resonances with positive binding energy up to $(j_1, j_2) = (1, 3)$ for J = 0, and up to $(j_1, j_2) = (2, 1)$ for J = 1 and 2.

We could find all the resonances that are expected from angular momentum addition rules. In columns 7 and 8 of Tables 8−10, we present the results of the GENIUSH-CAP computations with the W2CAP and W3CAP CAP functions; and these serve as reference values for the ETC method. We tested three polynomial CAP functions in the GENIUSH-CAP computations; the cusps corresponding to each function were usually close, the real and the imaginary parts of the energies usually agreed to better than 0.2 cm^{-1}. Note that we could not identify all cusps with all CAP functions. Even though the computations showed also some sensitivity to the functional form of the CAP, we could find all the resonances with a single value of the coordinate (r = 15 bohr) where the CAP is turned on, facilitating the determination of the resonances. Upon inspection of the energies, those states that share the same j_1, j_2, and L quantum numbers have very similar real energies. This confirms that the coupling of $\boldsymbol{J}_{12}$ with $\boldsymbol{L}$ and the parity of $|j_1 j_2 \pm\rangle$ have a small effect compared to the contribution of the dimers's end-to-end rotation. For a given dissociation channel, the lifetime of the resonances usually decreases with increasing energy. In some cases (e.g., for the (2, 0, 2, 1, 1) state with a negative binding energy) the imaginary part of the resonance energy is close to zero; thus, it cannot be determined precisely. The lifetime is a few hundred ps according to our resonance computations, but one should not take this number too literally

DOI: 10.1021/acs.jctc.9b00314
J. Chem. Theory Comput. 2019, 15, 4156−4169

Table 8. $J = 0$ Resonances with Positive Binding Energy[a]

						GENIUSH-CAP		ETC, $\eta = [5 \times 10^{-5}, 6 \times 10^{-5}]$			ETC, $\eta = [1.0 \times 10^{-4}, 1.1 \times 10^{-4}]$		
j_1	j_2	±	j_{12}	L	irrep	E	lifetime	E	lifetime	error %	E	lifetime	error %
1	1	+	2	2	B_1^+	238.7	3.4	239.0	3.0	13	239.0	3.0	14
2	0	+	2	2	A_1^+	356.0	3.9	356.3	3.3	20	356.3	3.3	20
2	1	±	2	2	E^-	473.8	19.1	473.7	18.1	6	473.7	18.0	6
2	1	±	3	3	E^+	477.7	1.1	478.1	1.1	7	478.1	1.1	7
3	0	±	3	3	E^+	710.1	1.4	710.4	1.3	10	710.5	1.3	11
2	2	+	2	2	A_1^+	710.3	4.7	710.5	3.6	32	710.4	3.6	32
2	2	−	3	3	B_1^-	713.5	1.1	714.0	1.0	8	714.1	1.0	7
2	2	+	4	4	A_1^+	716.8	0.5	719.7	0.5	16	719.3	0.5	19
3	1	+	2	2	B_1^+	825.9	3.6	826.0	3.1	16	825.9	3.2	14
3	1	+	3	3	B_2^-	828.1	2.1	828.2	1.9	10	828.2	1.9	12
3	1	−	3	3	A_1^-	828.8	1.2	829.2	1.1	7	829.3	1.1	7
3	1	+	4	4	B_1^+	832.1	0.6	834.7	0.5	10	834.4	0.5	11
3	1	−	4	4	A_2^+	834.1	0.5	835.1	0.4	6	834.6	0.4	8

[a] E is in cm^{-1}, and lifetime is in picoseconds.

Table 9. $J = 1$ Resonances with Positive Binding Energy[a]

						GENIUSH-CAP		ETC, $\eta = [5 \times 10^{-5}, 6 \times 10^{-5}]$			ETC, $\eta = [1.0 \times 10^{-4}, 1.1 \times 10^{-4}]$		
j_1	j_2	±	j_{12}	L	irrep	E	lifetime	E	lifetime	error %	E	lifetime	error %
1	0	±	1	2	E^-	119.5	12.6	119.5	12.2	3	119.5	13.2	4
1	1	−	1	2	A_2^+	237.1	265.5	237.1	343.2	23	237.1	300.0	12
1	1	+	2	2	B_1^+	238.2	8.9	238.1	6.4	40	238.1	7.2	23
1	1	+	2	3	B_2^-	241.8	1.1	242.1	1.0	7	242.3	1.0	7
2	0	+	2	1	A_2^-	352.6	156.2	352.6	212.2	26	352.6	382.3	59
2	0	+/−	2	2	A_1^+/B_2^+	354.7	126.4	354.7	124.8	1	354.7	126.4	0
2	0	−/+	2	2	B_2^+/A_1^+	355.9	5.1	356.1	3.8	35	356.0	3.7	36
2	0	−	2	3	B_1^-	358.9	1.5	359.0	1.3	12	359.1	1.3	15
2	0	+	2	3	A_2^-	359.1	1.1	359.5	1.1	7	359.6	1.1	7
2	1	±	1	2	E^-	473.6	15.1	473.6	12.4	22	473.6	13.8	9
2	1	±	2	2	E^-	474.0	16.3	474.0	14.0	16	474.0	15.5	5
2	1	±	3	2	E^-	474.4	4.9	474.6	3.6	37	474.6	3.6	38
2	1	±	2	3	E^+	477.3	1.6	477.5	1.4	13	477.5	1.4	16
2	1	±	3	3	E^+	477.6	1.1	478.0	1.0	8	478.1	1.0	9
2	1	±	3	4	E^-	480.9	0.5	483.7	0.5	13	483.8	0.4	22

[a] E is in cm^{-1}, and lifetime is in picoseconds.

due to the large relative error in the small imaginary part of the eigenvalue.

5.3.2. ETC Results. In columns 9−14 of Tables 8−10, we present the resonance energies obtained using the ETC method with two η_{guide} intervals and the DBSCAN clustering technique (see section 4.2.2). The energies correspond to the $(\langle x \rangle_i, \langle y \rangle_i)$ centroids of the resonance clusters identified. The clusters which appear in both η_{guide} calculations and have good variance scores are identified as resonances.

The results of the GENIUSH-CAP and the ETC computations agree reasonably well, the uncertainties of the results reflect the limitations of these techniques. Nonetheless, this agreement is much better than in a few cases where there can be an order of magnitude difference in the lifetimes computed with different methods. The agreement of the real part of the energies obtained with the ETC method and the original CAP method is better than 1 cm^{-1} if $L < 4$, and about 2−3 cm^{-1} for the $L = 4$ and 5 states. The agreement of the imaginary parts of the energies is a few tenth of cm^{-1} for $L < 4$, but the difference is larger if $L = 4$ or 5. We also present the percentage error of the ETC results as

$$\text{error \%} = \sqrt{\left(\frac{\mathrm{Re}(E)_{CAP} - \mathrm{Re}(E)_{ETC}}{\mathrm{Re}(E)_{CAP}}\right)^2 + \left(\frac{\mathrm{Im}(E)_{CAP} - \mathrm{Im}(E)_{ETC}}{\mathrm{Im}(E)_{CAP}}\right)^2} \times 100 \quad (20)$$

The percentage errors are dominated by the imaginary parts, as they are very small compared to the real part and a small variation causes large percentage errors.

The results obtained with the two η_{guide} ranges agree well. Nevertheless, it is important to try two η_{guide} ranges, as it helps to identify the resonance clusters. In most cases, the rectangular clustering and the DBSCAN algorithms result in very similar resonances. There are some minor differences, whereby the two clustering algorithms assign somewhat different points to the clusters. There were a few examples when we could identify a resonance cluster with DBSCAN but not with the rectangle clustering technique. In these cases the rectangular clustering technique could not find enough points of the resonance cluster, so the resonance was not identifiable. Overall, we recommend the use of the more robust DBSCAN technique.

DOI: 10.1021/acs.jctc.9b00314
J. Chem. Theory Comput. 2019, 15, 4156−4169

Table 10. $J = 2$ Resonances with Positive Binding Energy[a]

						GENIUSH-CAP		ETC, $\eta = [5 \times 10^{-5}, 6 \times 10^{-5}]$			ETC, $\eta = [1.0 \times 10^{-4}, 1.1 \times 10^{-4}]$		
j_1	j_2	±	j_{12}	L	irrep	E	lifetime	E	lifetime	error %	E	lifetime	error %
0	0	+	0	2	A_1^+	1.1	11.4	1.0	8.6	34	1.1	10.0	16
1	0	±	1	2	E^-	119.7	9.3	119.6	6.3	48	119.6	7.3	27
1	0	±	1	3	E^+	123.1	1.4	123.4	1.2	9	123.5	1.3	9
1	1	+	0	2	B_1^+	238.0	14.2	237.9	11.8	20	238.0	13.6	4
1	1	−	1	2	A_2^+	238.1	12.4	238.0	10.0	24	238.0	11.5	8
1	1	+	2	2	B_1^+	238.4	6.0	238.6	3.8	58	238.2	4.6	31
1	1	−	1	3	A_1^-	241.2	1.8	241.3	1.6	13	241.3	1.7	2
1	1	+	2	3	B_2^-	241.7	1.2	242.1	1.1	8	241.6	1.2	5
1	1	+	2	4	B_1^+	245.0	0.5	247.8	0.5	14	248.5	0.4	27
2	0	+	2	2	A_1^+	355.3	19.7	355.2	17.7	11	355.2	20.0	2
2	0	−	2	2	B_2^+	355.8	7.3	355.8	4.0	81	355.6	6.0	22
2	0	+	2	3	A_2^-	358.6	1.7	358.8	1.5	14	358.9	1.5	11
2	0	−	2	3	B_1^-	359.2	1.1	359.7	1.0	7	359.9	1.0	6
2	0	+	2	4	A_1^+	362.5	0.6	365.0	0.5	9	365.1	0.5	17
2	0	−	2	4	B_2^+	363.1	0.5	365.1	0.5	1	365.1	0.4	6
2	1	±	1	2	E^-	473.2	40.2	473.2	41.3	3	473.2	45.7	12
2	1	±	2	2	E^-	473.9	13.0	473.9	10.1	28	473.9	11.2	16
2	1	±	3	2	E^-	474.3	8.5	474.1	5.3	60	474.2	7.1	20
2	1	±	1	3	E^+	477.3	1.5	477.5	1.4	12	477.6	1.4	10
2	1	±	2	3	E^+	477.5	1.4	477.7	1.3	11	477.9	1.3	10
2	1	±	3	3	E^+	477.6	1.1	478.0	1.1	8	478.2	1.1	7
2	1	±	2	4	E^-	481.0	0.6	483.4	0.5	7	483.5	0.5	15
2	1	±	3	4	E^-	481.8	0.5	483.7	0.5	5	483.9	0.4	14
2	1	±	3	5	E^+	493.8	0.3	492.6	0.2	15	491.5	0.3	4

[a] E is in cm^{-1}, and lifetime is in picoseconds.

Table 11. GENIUSH-CAP Resonances Obtained with Two Different η Values Used in the ETC Method[a]

						CAP, $\eta = 5 \times 10^{-5}$			CAP, $\eta = 1.0 \times 10^{-4}$		
j_1	j_2	±	j_{12}	L	irrep	E	lifetime	error %	E	lifetime	error %
1	1	+	2	2	B_1^+	239.4	5.1	34	239.6	5.3	37
2	0	+	2	2	A_1^+	356.7	5.7	31	356.9	5.8	33
2	1	±	2	2	E^-	474.1	13.4	42	474.2	12.2	57
2	1	±	3	3	E^+	477.8	2.0	43	478.3	2.4	53
3	0	±	3	3	E^+	710.3	2.4	44	710.6	2.9	52
2	2	+	2	2	A_1^+	710.8	6.5	28	711.0	6.6	28
2	2	−	3	3	B_1^-	713.6	1.9	44	714.1	2.4	54
2	2	+	4	4	A_1^+	−	−	−	717.4	1.0	46
3	1	+	2	2	B_1^+	826.4	5.3	32	826.6	5.6	35
3	1	+	3	3	B_2^-	828.3	3.6	41	828.5	4.2	50
3	1	−	3	3	A_1^-	828.9	2.1	43	829.3	2.6	54
3	1	+	4	4	B_1^+	831.0	0.8	35	832.5	1.1	51
3	1	−	4	4	A_2^+	831.3	0.8	36	832.8	1.0	47

[a] E is in cm^{-1}, and lifetime is in picoseconds.

One may speculate that the good results of the ETC method are due to the choice of η_{guide} close to the η values corresponding to the cusps. However, this is definitely not the case: the η_{guide} values are larger than η at the cusps, as shown in Table 11. In Table 11, we present the $J = 0$ resonance eigenvalues of $\hat{H}(\eta) = \hat{H} - i\eta\hat{W}$, with $\eta = 5 \times 10^{-5}$ and 1×10^{-4}, and their errors. Except for two cases, when the errors are the same, these values are much farther from the GENIUSH-CAP resonances than the ETC resonances.

6. SUMMARY AND CONCLUSIONS

We have introduced an algorithm that makes the computation of resonance states within the complex absorption potential (CAP) technique almost automatic. In the original CAP technique, a CAP function is added to the Hamiltonian in order to damp the resonance wave functions so that basis functions used in bound-state computations can be utilized. The starting point of our algorithm is a method advocated by Tremblay and Carrington (TC).[26] In the TC method, use of certain eigenvectors of the CAP-perturbed Hamiltonian is recommended as a basis, and resonances can be determined as eigenvalues of the unperturbed Hamiltonian.

In the extended TC (ETC) method developed, we simplify the choice of the damped basis functions and establish stabilization criteria to identify resonance eigenvalues. To achieve this, we perform multiple computations with slightly different η_{guide} parameter values of the CAP-modified Hamiltonian, determine the resonance eigenvalues by clustering the

DOI: 10.1021/acs.jctc.9b00314
J. Chem. Theory Comput. 2019, 15, 4156−4169

complex eigenvalues, and then attach an appraisal score to the clusters.

We tested the performance of the ETC method on the rovibrational resonances of the $Ar{\cdot}NO^+$ and the $(H_2)_2$ complexes. The resonance states of the $Ar{\cdot}NO^+$ complex have been studied before with different techniques.[7] As part of this work, we have computed the low-lying resonances with the ETC method. The agreement between the results of the GENIUSH-CAP and ETC methods is good, though some resonances can be sensitive to the choice of the GENIUSH DVR basis functions.

Bound and resonance states of $(H_2)_2$ have been found in the proximity of the dissociation channels, corresponding to the rotational excitation of the H_2 monomers. Bound and negative binding energy resonance states for J = 0, 1, 2, and 3 were computed with the GENIUSH code. We found a few resonance states with negative binding energy that were not listed in the literature before. The resonance energies and lifetimes for J = 0, 1, and 2 were determined with both the GENIUSH-CAP code and the new ETC method, and they are in good agreement. We could find all the resonances of $(H_2)_2$ expected from angular momentum addition rules. Understanding the resonance states of $(H_2)_2$ may be beneficial in the real-gas thermochemistry of hydrogen, in the development of astrochemical models, and in the understanding and assignment of spectral transitions of $(H_2)_2$. In addition, it is straightforward to extend the present computations to the deuterated isotopologues of $(H_2)_2$ and to other complexes, as well.

The results of a number of careful tests show that the ETC method is an effective semi-automatic technique to compute rovibrational resonance states. The ETC method results in similar resonances as the original CAP technique but with much less human effort and in a much more objective manner.

AUTHOR INFORMATION

Corresponding Author

*E-mail: csaszarag@caesar.elte.hu.

ORCID

Tamás Szidarovszky: 0000-0003-0878-5212

Attila G. Császár: 0000-0001-5640-191X

Notes

The authors declare no competing financial interest.

ACKNOWLEDGMENTS

This work received support from NKFIH (grants no. K119658 and PD124623) and from the grant VEKOP-2.3.2-16-2017-00014 supported by the European Union and the State of Hungary and co-financed by the European Regional Development Fund. The authors are grateful to Prof. Carrington for pointing out ref 26 to them.

REFERENCES

(1) Maksyutenko, P.; Rizzo, T. R.; Boyarkin, O. V. A direct measurement of the dissociation energy of water. *J. Chem. Phys.* **2006**, *125*, 181101.

(2) Furtenbacher, T.; Szidarovszky, T.; Hrubý, J.; Kyuberis, A. A.; Zobov, N. F.; Polyansky, O. L.; Tennyson, J.; Császár, A. G. Definitive high-temperature ideal-gas thermochemical functions of the $H_2{}^{16}O$ molecule. *J. Phys. Chem. Ref. Data* **2016**, *45*, 043104.

(3) Simkó, I.; Furtenbacher, T.; Dénes, N.; Szidarovszky, T.; Hrubý, J.; Zobov, N. F.; Polyansky, O. L.; Tennyson, J.; Császár, A. G.; Gamache, R. R. Recommended ideal-gas thermochemical functions for heavy water and its substituent isotopologues. *J. Phys. Chem. Ref. Data* **2017**, *46*, 023104.

(4) Császár, A. G.; Fábri, C.; Szidarovszky, T.; Mátyus, E.; Furtenbacher, T.; Czakó, G. Fourth age of quantum chemistry: Molecules in motion. *Phys. Chem. Chem. Phys.* **2012**, *14*, 1085−1106.

(5) Tennyson, J.; Kostin, M. A.; Barletta, P.; Harris, G. J.; Polyansky, O. L.; Ramanlal, J.; Zobov, N. F. DVR3D: a program suite for the calculation of rotation-vibration spectra of triatomic molecules. *Comput. Phys. Commun.* **2004**, *163*, 85−116.

(6) Bowman, J. M.; Carrington, T.; Meyer, H.-D. Variational quantum approaches for computing vibrational energies of polyatomic molecules. *Mol. Phys.* **2008**, *106*, 2145−2182.

(7) Papp, D.; Sarka, J.; Szidarovszky, T.; Császár, A. G.; Mátyus, E.; Hochlaf, M.; Stoecklin, T. Complex rovibrational dynamics of the $Ar{\cdot}NO^+$ complex. *Phys. Chem. Chem. Phys.* **2017**, *19*, 8152−8160.

(8) Reinhardt, W. P. Complex coordinates in the theory of atomic and molecular structure and dynamics. *Annu. Rev. Phys. Chem.* **1982**, *33*, 223−255.

(9) Riss, U. V.; Meyer, H. D. Calculation of resonance energies and widths using the complex absorbing potential method. *J. Phys. B: At., Mol. Opt. Phys.* **1993**, *26*, 4503−4536.

(10) Mandelshtam, V.; Moiseyev, N. Complex scaling of ab initio molecular potential surfaces. *J. Chem. Phys.* **1996**, *104*, 6192−6195.

(11) Moiseyev, N. *Non-Hermitian Quantum Mechanics*; Cambridge University Press, 2011;.

(12) Silva, B. C.; Barletta, P.; Munro, J. J.; Tennyson, J. Resonant states of H_3^+ and D_2H^+. *J. Chem. Phys.* **2008**, *128*, 244312.

(13) Mandelshtam, V. A.; Ravuri, T. R.; Taylor, H. S. Calculation of the density of resonance states using the stabilization method. *Phys. Rev. Lett.* **1993**, *70*, 1932−1935.

(14) Taylor, J. R. *Scattering Theory*; Wiley: New York, 1972.

(15) Watanabe, A.; Welsh, H. L. Direct spectroscopic evidence of bound states of $(H_2)_2$ complexes at low temperatures. *Phys. Rev. Lett.* **1964**, *13*, 810−812.

(16) McKellar, A. R. W. Experimental verification of hydrogen dimers in the atmospheres of Jupiter and Saturn from Voyager IRIS far-infrared spectra. *Astrophys. J.* **1988**, *326*, L75−L77.

(17) McKellar, A. R. W. Infrared spectra of hydrogen dimers. *J. Chem. Phys.* **1990**, *92*, 3261−3277.

(18) McKellar, A. R. W.; Schaefer, J. Far infrared spectra of hydrogen dimers: Comparisons of experiment and theory for $(H_2)_2$ and $(D_2)_2$ at 20 K. *J. Chem. Phys.* **1991**, *95*, 3081−3091.

(19) McKellar, A. R. W. Long-path equilibrium IR spectra of weakly bound complexes at low temperatures. *Faraday Discuss.* **1994**, *97*, 69−80.

(20) Tejeda, G.; Fernández, J. M.; Montero, S.; Blume, D.; Toennies, J. P. Raman spectroscopy of small *para*-H_2 clusters formed in cryogenic free jets. *Phys. Rev. Lett.* **2004**, *92*, 223401.

(21) Papp, D.; Szidarovszky, T.; Császár, A. G. A general variational approach for computing rovibrational resonances of polyatomic molecules. Application to the weakly bound H_2He^+ and H_2CO systems. *J. Chem. Phys.* **2017**, *147*, 094106.

(22) Harris, D. O.; Engerholm, G. G.; Gwinn, W. D. Calculation of matrix elements for one-dimensional quantum-mechanical problems and the application to anharmonic oscillators. *J. Chem. Phys.* **1965**, *43*, 1515−1517.

(23) Szalay, V. Discrete variable representations of differential operators. *J. Chem. Phys.* **1993**, *99*, 1978−1984.

(24) Mátyus, E.; Czakó, G.; Császár, A. G. Toward black-box-type full- and reduced-dimensional variational (ro)vibrational computations. *J. Chem. Phys.* **2009**, *130*, 134112.

(25) Fábri, C.; Mátyus, E.; Császár, A. G. Rotating full- and reduced-dimensional quantum chemical models of molecules. *J. Chem. Phys.* **2011**, *134*, 074105.

(26) Tremblay, J.; Carrington, T. Computing resonance energies, widths, and wave functions using a Lanczos method in real arithmetic. *J. Chem. Phys.* **2005**, *122*, 244107.

(27) Ester, M.; Kriegel, H.-P.; Sander, J.; Xu, X. A density-based algorithm for discovering clusters in large spatial databases with noise. *KDD'96*, Proceedings of the Second International Conference on

DOI: 10.1021/acs.jctc.9b00314
J. Chem. Theory Comput. 2019, 15, 4156−4169

Knowledge Discovery and Data Mining, Portland, OR, Aug 2−4, 1996; pp 226−231.
(28) Poirier, B.; Carrington, T. Semiclassically optimized complex absorbing potentials of polynomial form I. Pure imaginary case. *J. Chem. Phys.* **2003**, *118*, 17−28.
(29) Papp, D.; Császár, A. G.; Yamanouchi, K.; Szidarovszky, T. Rovibrational resonances in H_2He^+. *J. Chem. Theory Comput.* **2018**, *14*, 1523−1533.
(30) Frommhold, L.; Samuelson, R.; Birnbaum, G. Hydrogen dimer structures in the far-infrared spectra of Jupiter and Saturn. *Astrophys. J.* **1984**, *283*, L79−L82.
(31) McKellar, A. R. W. Possible identification of sharp features in the Voyager far-infrared spectra of Jupiter and Saturn. *Can. J. Phys.* **1984**, *62*, 760−763.
(32) Gordon, R. G.; Cashion, J. K. Intermolecular potentials and the infrared spectrum of the molecular complex $(H_2)_2$. *J. Chem. Phys.* **1966**, *44*, 1190−1195.
(33) Schaefer, J.; Meyer, W. Theoretical studies of H_2-H_2 collisions. I. Elastic scattering of ground state para- and ortho-H_2 in the rigid rotor approximation. *J. Chem. Phys.* **1979**, *70*, 344−360.
(34) Danby, G.; Flower, D. R. On the $S_0(0)$ and $S_1(0)$ spectra of the H_2−H_2 dimer. *J. Chem. Phys. B: At. Mol. Phys.* **1984**, *17*, L867−L870.
(35) Schaefer, J. Empirical corrections of the rigid rotor interaction potential of H_2−H_2 in the attractive region: Dimer features in the FIR absorption spectra. *Astron. Astrophys.* **1994**, *284*, 1015−1025.
(36) Bunker, P. R. Symmetry in $(H_2)_2$, $(D_2)_2$, $(HD)_2$, and H_2-D_2 van der Waals complexes. *Can. J. Phys.* **1979**, *57*, 2099−2105.
(37) Bunker, P. R.; Jensen, P. *Molecular Symmetry and Spectroscopy*; NRC Research Press: Ottawa, 1998.
(38) Hinde, R. J. A six-dimensional H_2-H_2 potential energy surface for bound state spectroscopy. *J. Chem. Phys.* **2008**, *128*, 154308.
(39) Szidarovszky, T.; Császár, A. G.; Czakó, G. On the efficiency of treating singularities in triatomic variational vibrational computations. The vibrational states of H_3^+ up to dissociation. *Phys. Chem. Chem. Phys.* **2010**, *12*, 8373−8386.
(40) Meyer, R. Trigonometric interpolation method for one-dimensional quantum mechanical problems. *J. Chem. Phys.* **1970**, *52*, 2053−2059.
(41) http://www.sourceforge.net/projects/lapackpp.
(42) Halvick, P.; Stoecklin, T.; Lique, F.; Hochlaf, M. Explicitly correlated treatment of the Ar-NO^+ cation. *J. Chem. Phys.* **2011**, *135*, 044312.
(43) Light, J. C.; Carrington, T. Discrete variable representations and their utilization. *Adv. Chem. Phys.* **2007**, *114*, 263−310.
(44) Le Roy, R. J.; Hutson, J. M. Improved potential energy surfaces for the interaction of H_2 with Ar, Kr, and Xe. *J. Chem. Phys.* **1987**, *86*, 837−853.
(45) Stoicheff, B. P. High resolution Raman spectroscopy of gases: IX. Spectra of H_2, HD, and D_2. *Can. J. Phys.* **1957**, *35*, 730−741.
(46) Theil, H. A Rank-Invariant Method of Linear and Polynomial Regression Analysis. *Proc. Koninklijke Nederlandse Akad. Wetenschappen, Ser. A - Math. Sci.* **1950**, *53*, 386−392.
(47) Sen, P. K. Estimates of the regression coefficient based on Kendall's tau. *J. Am. Stat. Assoc.* **1968**, *63*, 1379−1389.
(48) Stanton, J. F.; Gauss, J.; Cheng, L.; Harding, M. E.; Matthews, D. A.; Szalay, P. G. *CFOUR, a quantum chemical program package*, with contributions from Auer, A. A., Bartlett, R. J., Benedikt, U., Berger, C., Bernholdt, D. E., Bomble, Y. J., Christiansen, O., Engel, F., Faber, R., Heckert, M., Heun, O., Huber, C., Jagau, T.-C., Jonsson, D., Jusélius, J., Klein, K., Lauderdale, W. J., Lipparini, F., Metzroth, T., Mück, L. A., O'Neill, D. P., Price, D. R., Prochnow, E., Puzzarini, C. Ruud, K. Schiffmann, F., Schwalbach, W., Simmons, C., Stopkowicz, S., Tajti, A., Vázquez, J., Wang, F., Watts, J. D., and the integral packages MOLECULE (Almlöf, J., and Taylor, P. R.), PROPS (Taylor, P. R.), ABACUS (Helgaker, T., Jensen, H. J. Aa., Jørgensen, P., and Olsen, J.), and ECP routines by Mitin, A. V., and van Wüllen, C. For the current version, see: http://www.cfour.de.
(49) Dunning, T. H., Jr. Gaussian basis sets for use in correlated molecular calculations. I. The atoms boron through neon and hydrogen. *J. Chem. Phys.* **1989**, *90*, 1007−1023.
(50) Foltz, J. V.; Rank, D. H.; Wiggins, T. A. Determinations of some hydrogen molecular constants. *J. Mol. Spectrosc.* **1966**, *21*, 203−216.
(51) https://webbook.nist.gov/cgi/cbook.cgi?ID=C1333740.

DOI: 10.1021/acs.jctc.9b00314
J. Chem. Theory Comput. 2019, 15, 4156−4169